Electronic Supplementary Material (ESI) for Physical Chemistry Chemical Physics.

Support information: Thermoelectric power factor of doped Bi_2O_2Se: A computational study

Kerong Hu[a], Jian Han[a], Ben Xu[a,*] and Yuan-Hua Lin[a]

[a]*School of Materials Science and Engineering, Tsinghua University, Beijing 100084, China*

Corresponding author: Ben Xu

E-mail:xuben@mail.tsinghua.edu.cn

1. Crystal structure and band structure

Bi_2O_2Se crystallizes into a body-centered tetragonal structure with the space group of I4/mmm. Unlike other layered materials which have individual atomic layers stacked by van der Waals interaction, Bi_2O_2Se lacks a well-defined van der Waals gap but displays electrostatic interaction[1] along c-axis between tetragonal diatomic $[Bi_2O_2]^{2+}$ layer and monoatomic $[Se]^{2-}$ layer, as shown in Fig. 1. The calculation for the pristine Bi_2O_2Se was carried out on the primitive cell. The calculated lattice constants are slightly larger than the experimental values. It can ascribe to the fact that GGA often overestimated the lattice parameters of solids. The errors are within 2%, which are good agreement with the experiment. Table 1 shows the relaxed lattice constant and band gap for the pristine Bi_2O_2Se and compares to the other results.

The calculated band gap shows a large deviation from 0.41 to 1.01 eV, and the experiment was reported as 0.8 eV. The band structure we calculated is based on primitive cells, but other literature reports are based on unit cells. The reason for using primitive cells is that half of the atoms are required for modeling under the same carrier concentration, which can save computing resources. But the result is comparable. Fig. 2 displays the calculated band structure based on primitive cell and unit cell and their corresponding Brillouin zone.

All the calculation results have a similar dispersion tendency, but our result shows that the energy of the conduction band is lower than other results. All the results show that the VBM is located at point X and there exists a local maximum at point R. As for CBM, all the results are located at point Gamma, where is a good agreement with our primitive cell result. The difference between our calculation and TB-mBJ GGA is the degeneracy of the conduction band at point A. However, it has the same behavior as HSE06, which both converges at point A.

To balance our main purpose and the calculation resource, the relative changes of band structure near the Fermi level are required. Although the band gap is underestimated, the dispersion relationship calculated by PBE is credible.

Table 1. The comparison of the lattice constant and band gap of pristine Bi2O2Se between this work and reported literatures.

phase	method	a (Å)	c (Å)	E_g (eV)
Bi_2O_2Se	PBE, this work	3.93	12.41	0.41
	TBmBJ-GGA[2]	3.92	12.40	0.87
	HSE06[3]	3.92	12.39	1.01
	Experiment[4]	3.88	12.16	0.80

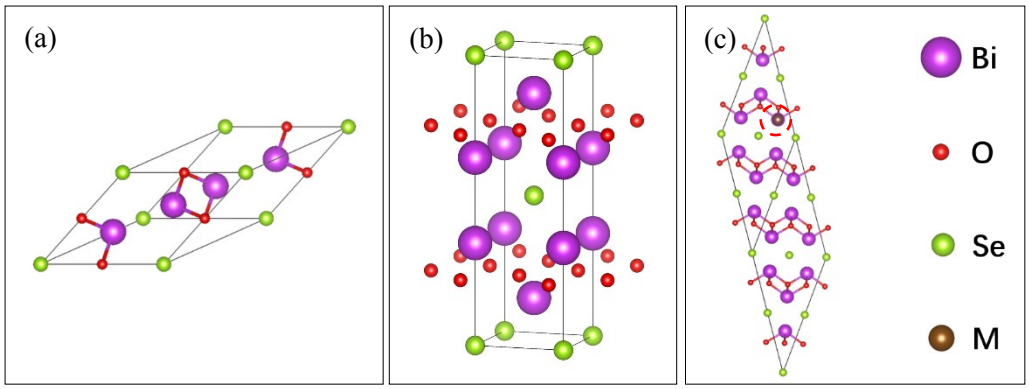

Figure 1. The crystal structure of (a) primitive cell, (b) unit cell and (c) supercell Bi_2O_2Se, where the purple circle denotes the Bi atom, red circle denotes the O atom, green circle denotes the Se atom, and the brown circle denotes the doping elements.

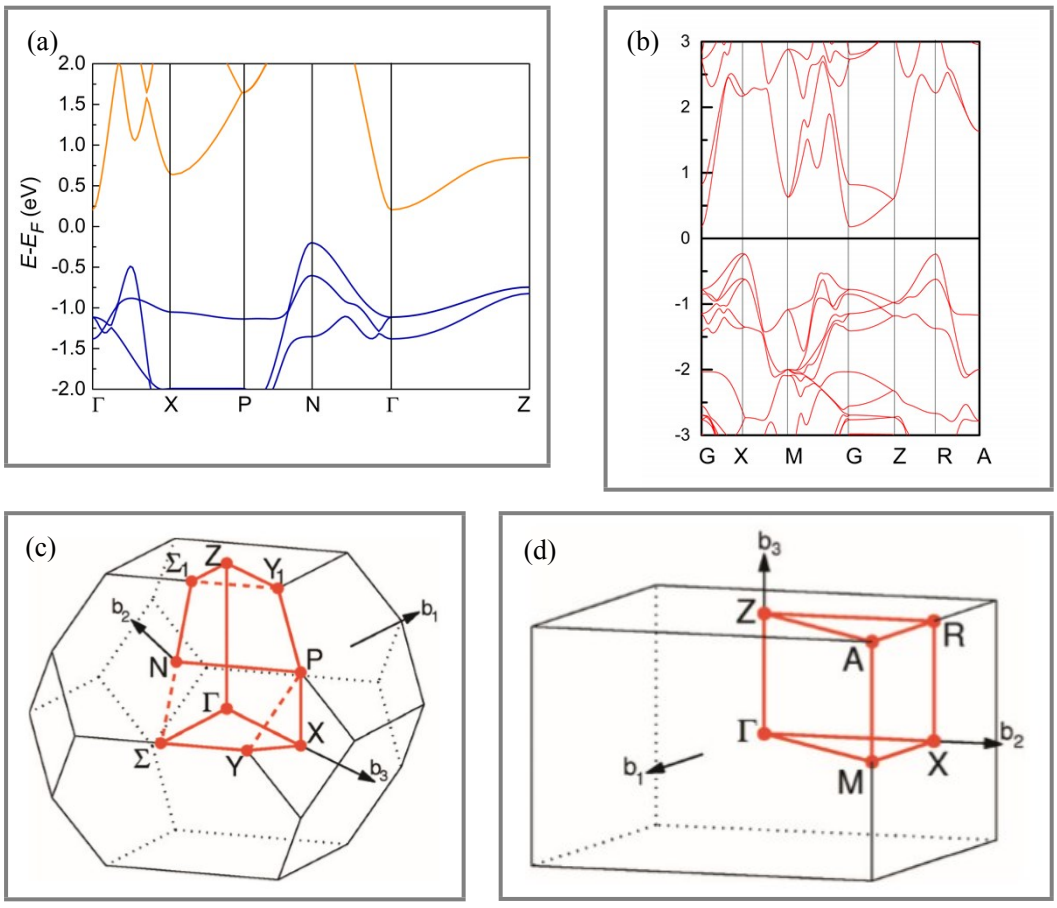

Figure 2. The calculated band structure of (a) primitive cell and (b) unit cell of Bi2O2Se, (c) and (d) are the corresponding Brillouin zone.

2. Experimental data of the Seebeck coefficient and electrical conductivity from literature

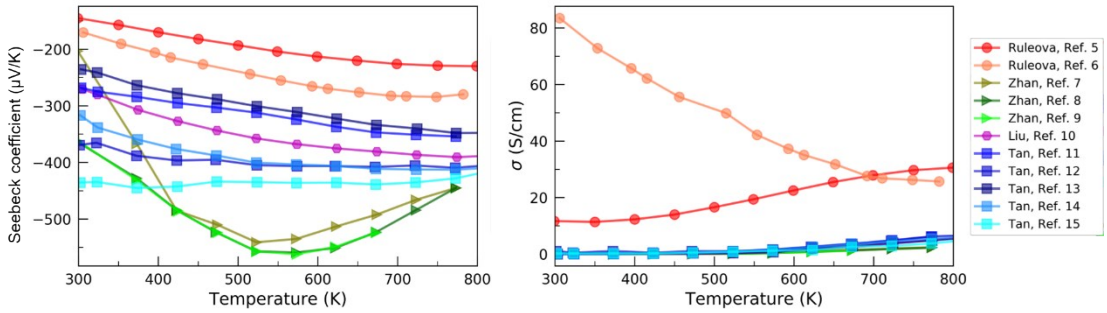

Figure 3. The experimental data of (a) Seebeck coefficient and (b) electrical conductivity from literature.

3. Projected density of states

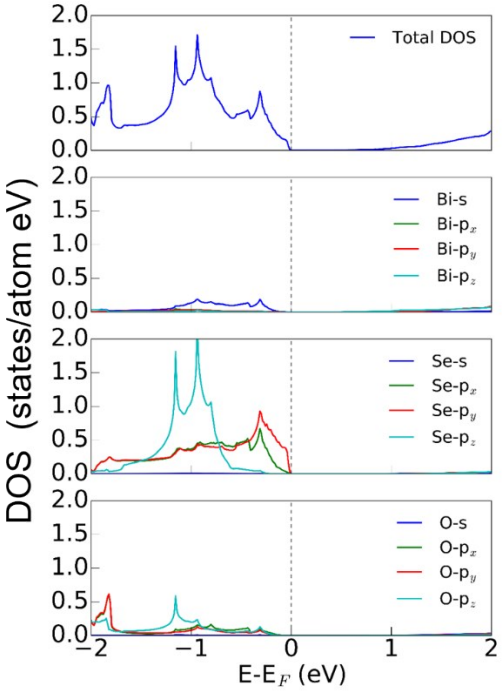

(a)

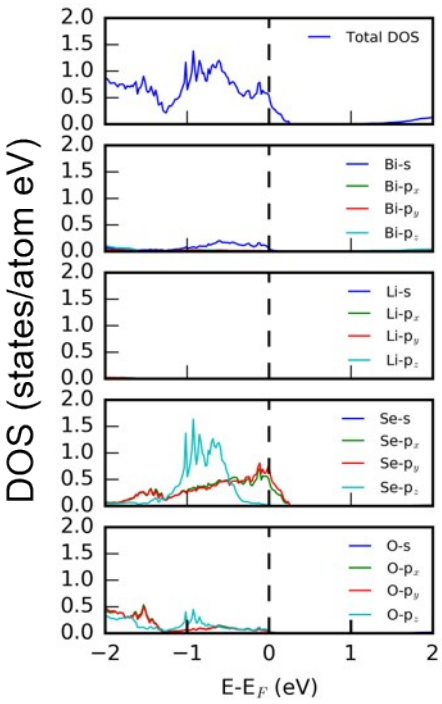

(b)

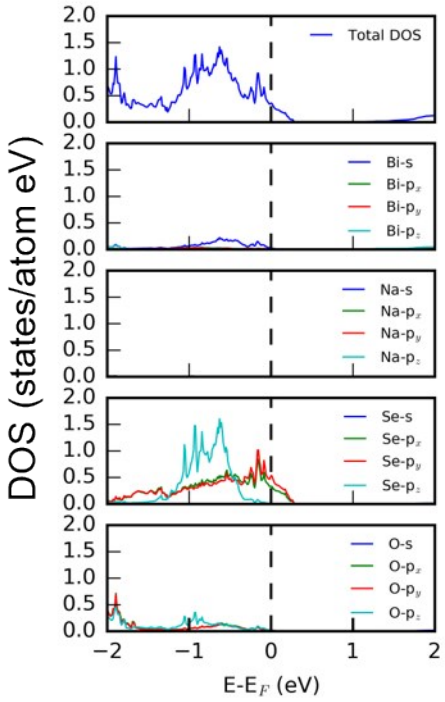

(c)

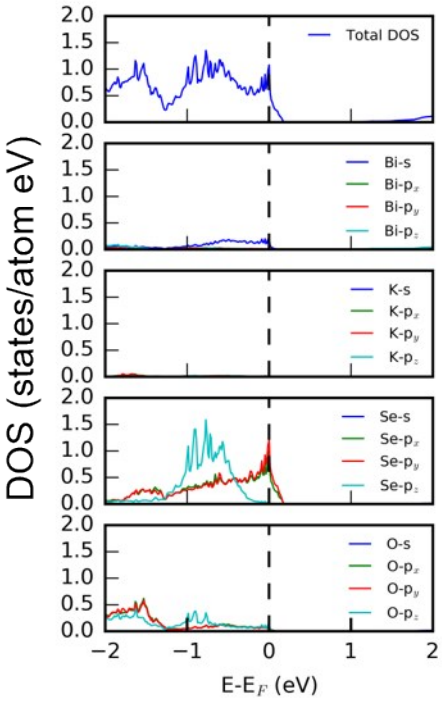

(d)

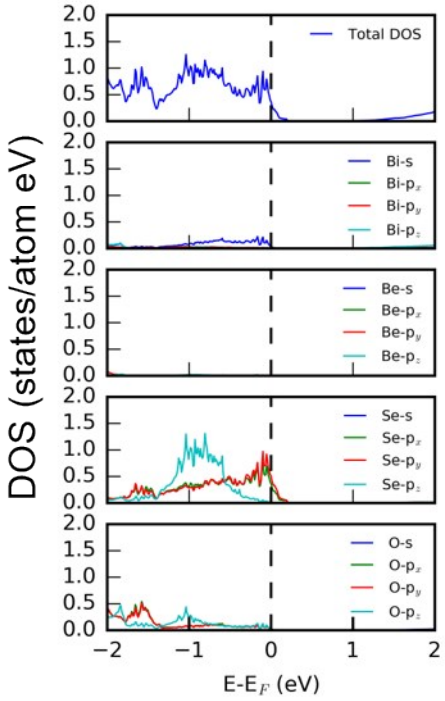
DOS (states/atom eV)
Total DOS
Bi-s
Bi-p$_x$
Bi-p$_y$
Bi-p$_z$
Be-s
Be-p$_x$
Be-p$_y$
Be-p$_z$
Se-s
Se-p$_x$
Se-p$_y$
Se-p$_z$
O-s
O-p$_x$
O-p$_y$
O-p$_z$
E-E$_F$ (eV)

(e)

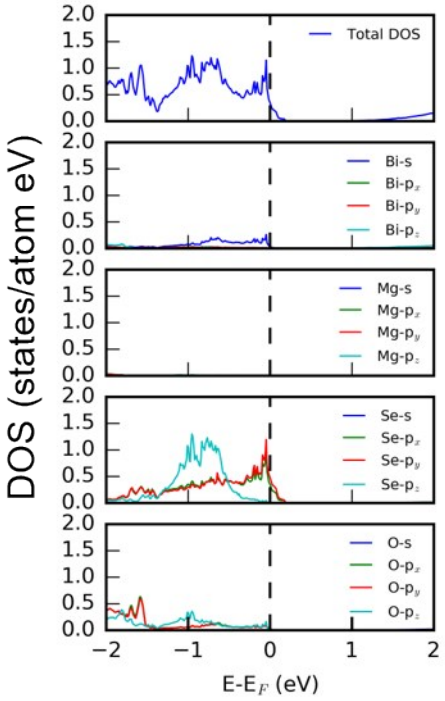
DOS (states/atom eV)
Total DOS
Bi-s
Bi-p$_x$
Bi-p$_y$
Bi-p$_z$
Mg-s
Mg-p$_x$
Mg-p$_y$
Mg-p$_z$
Se-s
Se-p$_x$
Se-p$_y$
Se-p$_z$
O-s
O-p$_x$
O-p$_y$
O-p$_z$
E-E$_F$ (eV)

(f)

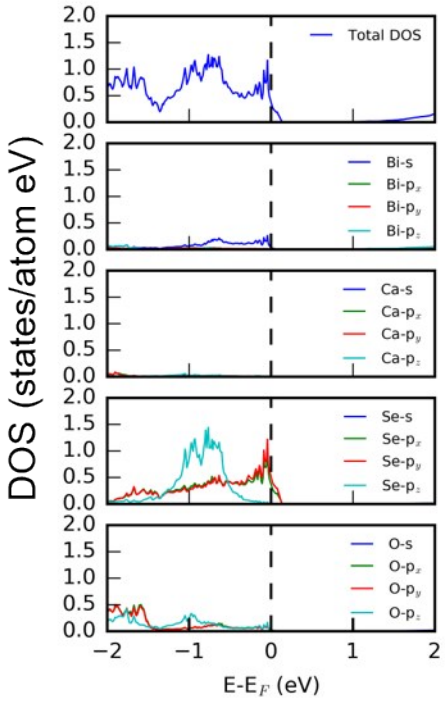
DOS (states/atom eV)
Total DOS
Bi-s
Bi-p$_x$
Bi-p$_y$
Bi-p$_z$
Ca-s
Ca-p$_x$
Ca-p$_y$
Ca-p$_z$
Se-s
Se-p$_x$
Se-p$_y$
Se-p$_z$
O-s
O-p$_x$
O-p$_y$
O-p$_z$
E-E$_F$ (eV)

(g)

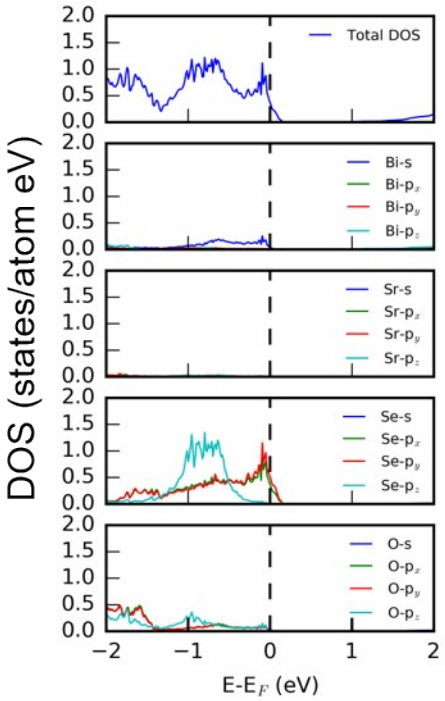
DOS (states/atom eV)
Total DOS
Bi-s
Bi-p$_x$
Bi-p$_y$
Bi-p$_z$
Sr-s
Sr-p$_x$
Sr-p$_y$
Sr-p$_z$
Se-s
Se-p$_x$
Se-p$_y$
Se-p$_z$
O-s
O-p$_x$
O-p$_y$
O-p$_z$
E-E$_F$ (eV)

(h)

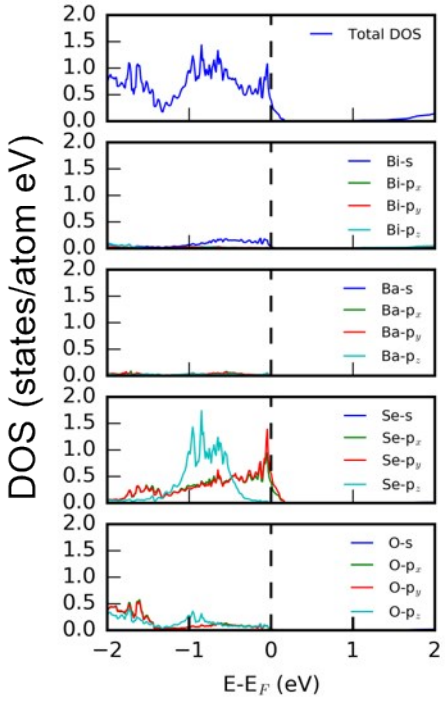
DOS (states/atom eV)
Total DOS
Bi-s
Bi-p$_x$
Bi-p$_y$
Bi-p$_z$
Ba-s
Ba-p$_x$
Ba-p$_y$
Ba-p$_z$
Se-s
Se-p$_x$
Se-p$_y$
Se-p$_z$
O-s
O-p$_x$
O-p$_y$
O-p$_z$
E-E$_F$ (eV)

(i)

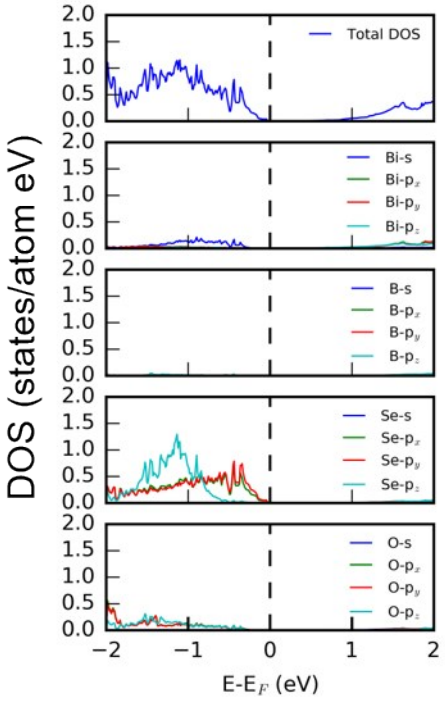
DOS (states/atom eV)
Total DOS
Bi-s
Bi-p$_x$
Bi-p$_y$
Bi-p$_z$
B-s
B-p$_x$
B-p$_y$
B-p$_z$
Se-s
Se-p$_x$
Se-p$_y$
Se-p$_z$
O-s
O-p$_x$
O-p$_y$
O-p$_z$
E-E$_F$ (eV)

(j)

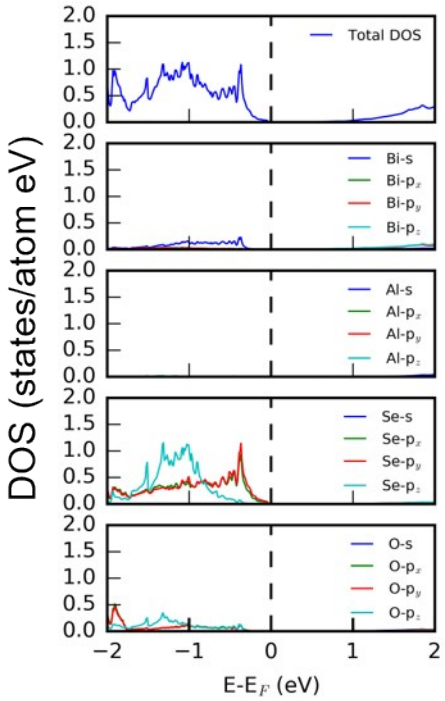
DOS (states/atom eV)
Total DOS
Bi-s
Bi-p$_x$
Bi-p$_y$
Bi-p$_z$
Al-s
Al-p$_x$
Al-p$_y$
Al-p$_z$
Se-s
Se-p$_x$
Se-p$_y$
Se-p$_z$
O-s
O-p$_x$
O-p$_y$
O-p$_z$
E-E$_F$ (eV)

(k)

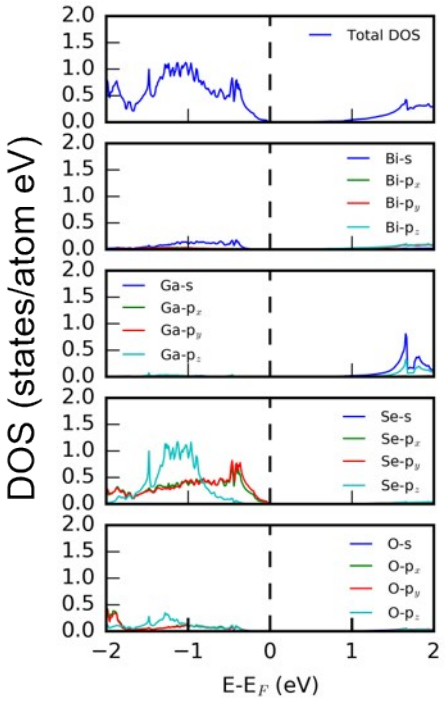
DOS (states/atom eV)
Total DOS
Bi-s
Bi-p$_x$
Bi-p$_y$
Bi-p$_z$
Ga-s
Ga-p$_x$
Ga-p$_y$
Ga-p$_z$
Se-s
Se-p$_x$
Se-p$_y$
Se-p$_z$
O-s
O-p$_x$
O-p$_y$
O-p$_z$
E-E$_F$ (eV)

(l)

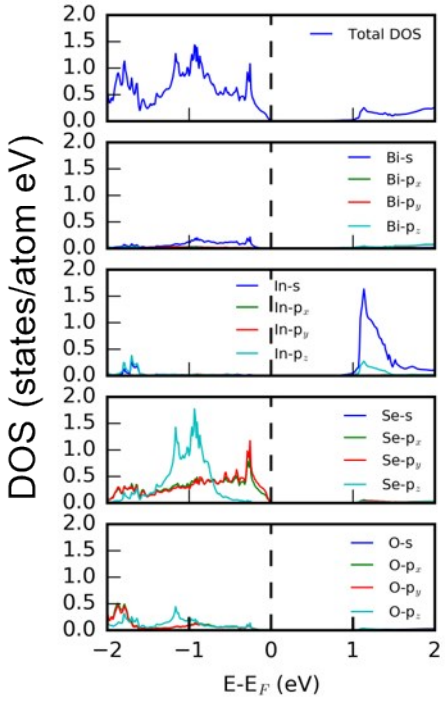
DOS (states/atom eV)
Total DOS
Bi-s
Bi-p$_x$
Bi-p$_y$
Bi-p$_z$
In-s
In-p$_x$
In-p$_y$
In-p$_z$
Se-s
Se-p$_x$
Se-p$_y$
Se-p$_z$
O-s
O-p$_x$
O-p$_y$
O-p$_z$
E-E$_F$ (eV)

(m)

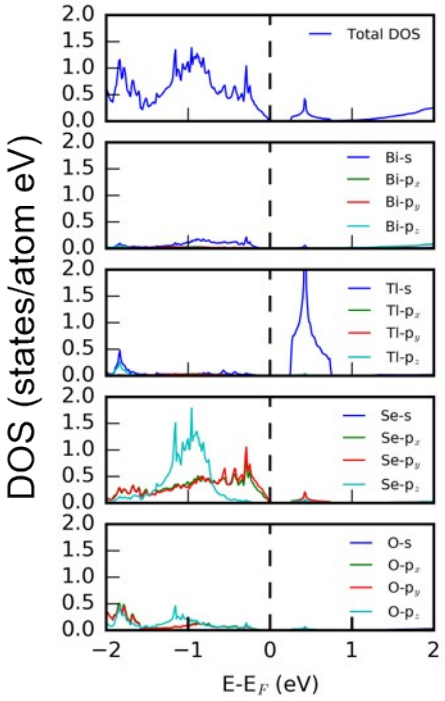
DOS (states/atom eV)
Total DOS
Bi-s
Bi-p$_x$
Bi-p$_y$
Bi-p$_z$
Tl-s
Tl-p$_x$
Tl-p$_y$
Tl-p$_z$
Se-s
Se-p$_x$
Se-p$_y$
Se-p$_z$
O-s
O-p$_x$
O-p$_y$
O-p$_z$
E-E$_F$ (eV)

(n)

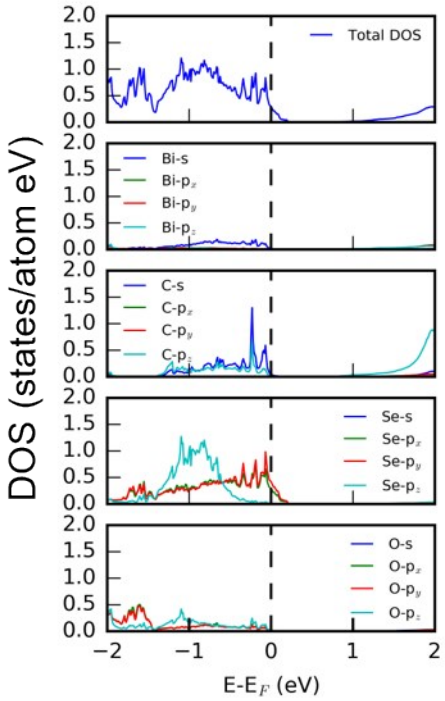
DOS (states/atom eV)
Total DOS
Bi-s
Bi-p$_x$
Bi-p$_y$
Bi-p$_z$
C-s
C-p$_x$
C-p$_y$
C-p$_z$
Se-s
Se-p$_x$
Se-p$_y$
Se-p$_z$
O-s
O-p$_x$
O-p$_y$
O-p$_z$
E-E$_F$ (eV)

(o)

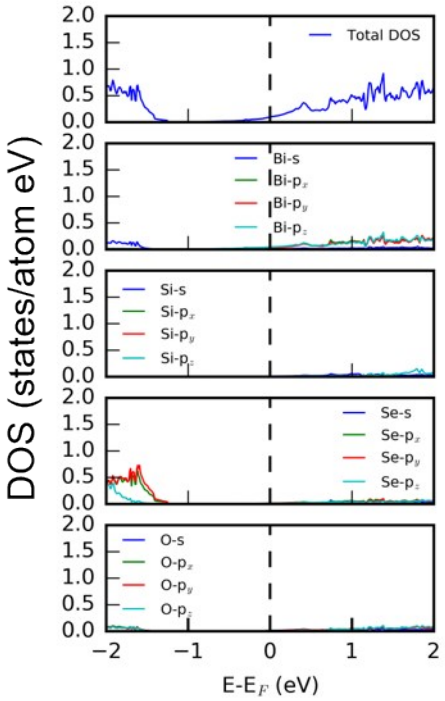
DOS (states/atom eV)
Total DOS
Bi-s
Bi-p$_x$
Bi-p$_y$
Bi-p$_z$
Si-s
Si-p$_x$
Si-p$_y$
Si-p$_z$
Se-s
Se-p$_x$
Se-p$_y$
Se-p$_z$
O-s
O-p$_x$
O-p$_y$
O-p$_z$
E-E$_F$ (eV)

(p)

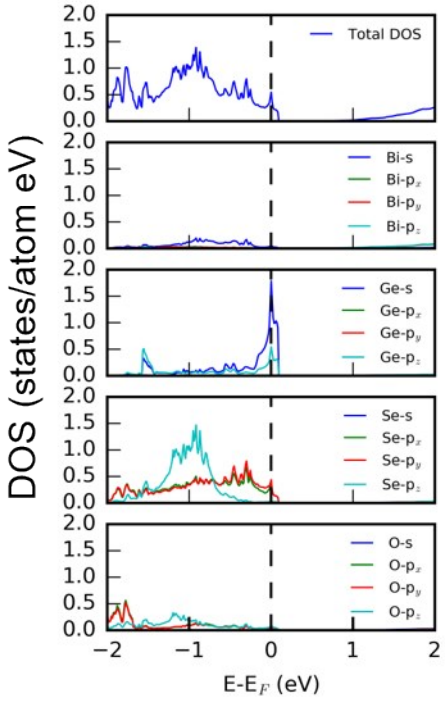
Total DOS
Bi-s
Bi-p$_x$
Bi-p$_y$
Bi-p$_z$
Ge-s
Ge-p$_x$
Ge-p$_y$
Ge-p$_z$
Se-s
Se-p$_x$
Se-p$_y$
Se-p$_z$
O-s
O-p$_x$
O-p$_y$
O-p$_z$
DOS (states/atom eV)
E-E$_F$ (eV)

(q)

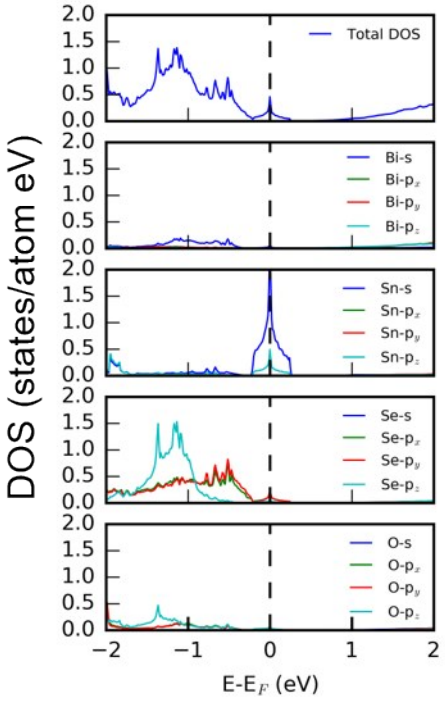
Total DOS
Bi-s
Bi-p$_x$
Bi-p$_y$
Bi-p$_z$
Sn-s
Sn-p$_x$
Sn-p$_y$
Sn-p$_z$
Se-s
Se-p$_x$
Se-p$_y$
Se-p$_z$
O-s
O-p$_x$
O-p$_y$
O-p$_z$
DOS (states/atom eV)
E-E$_F$ (eV)

(r)

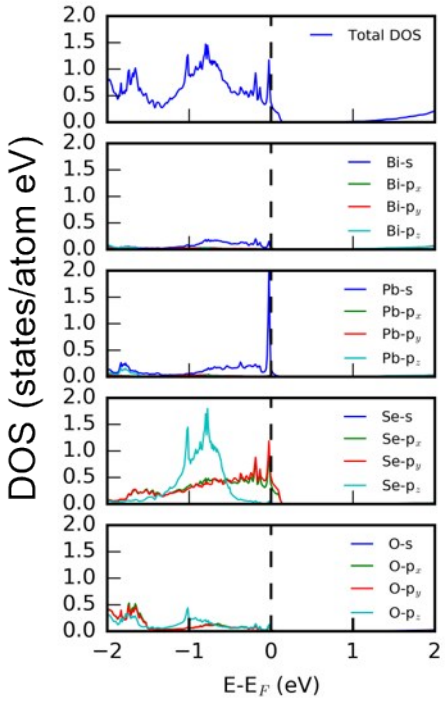
Total DOS
Bi-s
Bi-p$_x$
Bi-p$_y$
Bi-p$_z$
Pb-s
Pb-p$_x$
Pb-p$_y$
Pb-p$_z$
Se-s
Se-p$_x$
Se-p$_y$
Se-p$_z$
O-s
O-p$_x$
O-p$_y$
O-p$_z$
DOS (states/atom eV)
E-E$_F$ (eV)

(s)

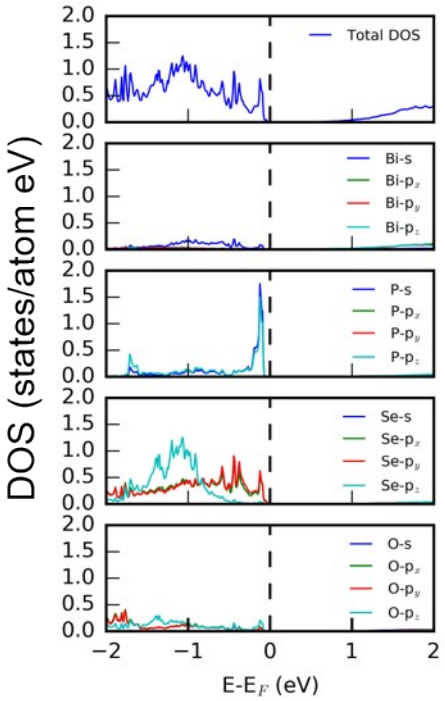
Total DOS
Bi-s
Bi-p$_x$
Bi-p$_y$
Bi-p$_z$
P-s
P-p$_x$
P-p$_y$
P-p$_z$
Se-s
Se-p$_x$
Se-p$_y$
Se-p$_z$
O-s
O-p$_x$
O-p$_y$
O-p$_z$
DOS (states/atom eV)
E-E$_F$ (eV)

(t)

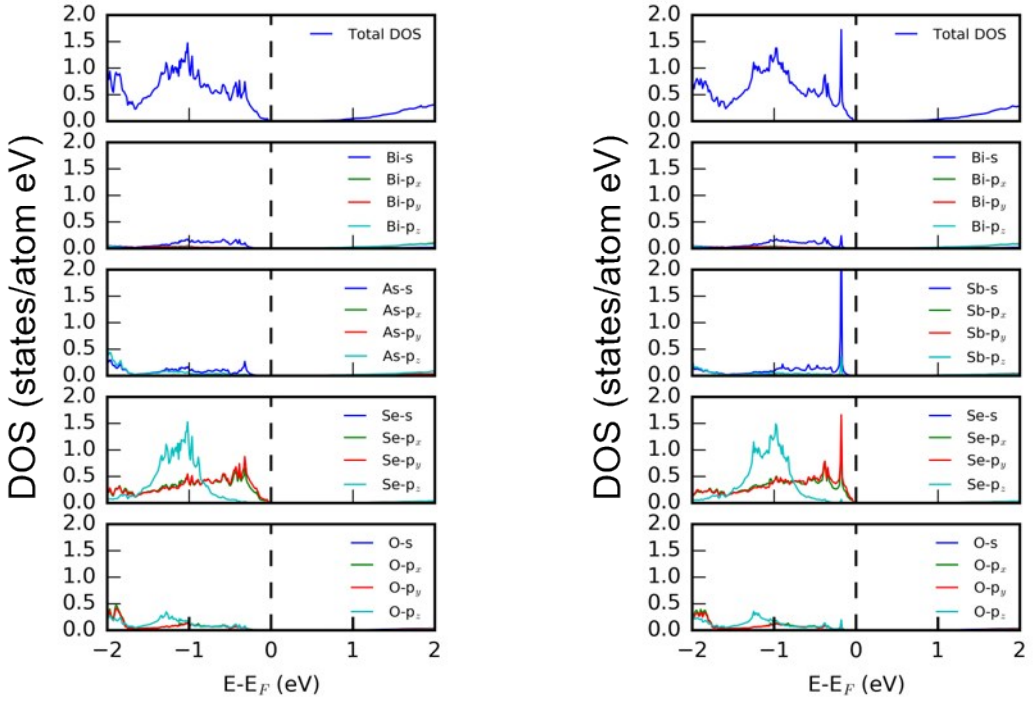

(u) (v)

Figure 4. The calculated projected density of states (PDOS) for pristine Bi_2O_2Se (a) and the doping cases, from (b) to (v) are (b) Li, (c) Na, (d) K, (e) Be, (f) Mg, (g) Ca, (h) Sr, (i) Ba, (j) B, (k) Al, (l) Ga, (m) In, (n) Tl, (o) C, (p) Si, (q) Ge, (r) Sn, (s) Pb, (t) P, (u) As, (v) Sb doping respectively.

4. Calculated electrical conductivity

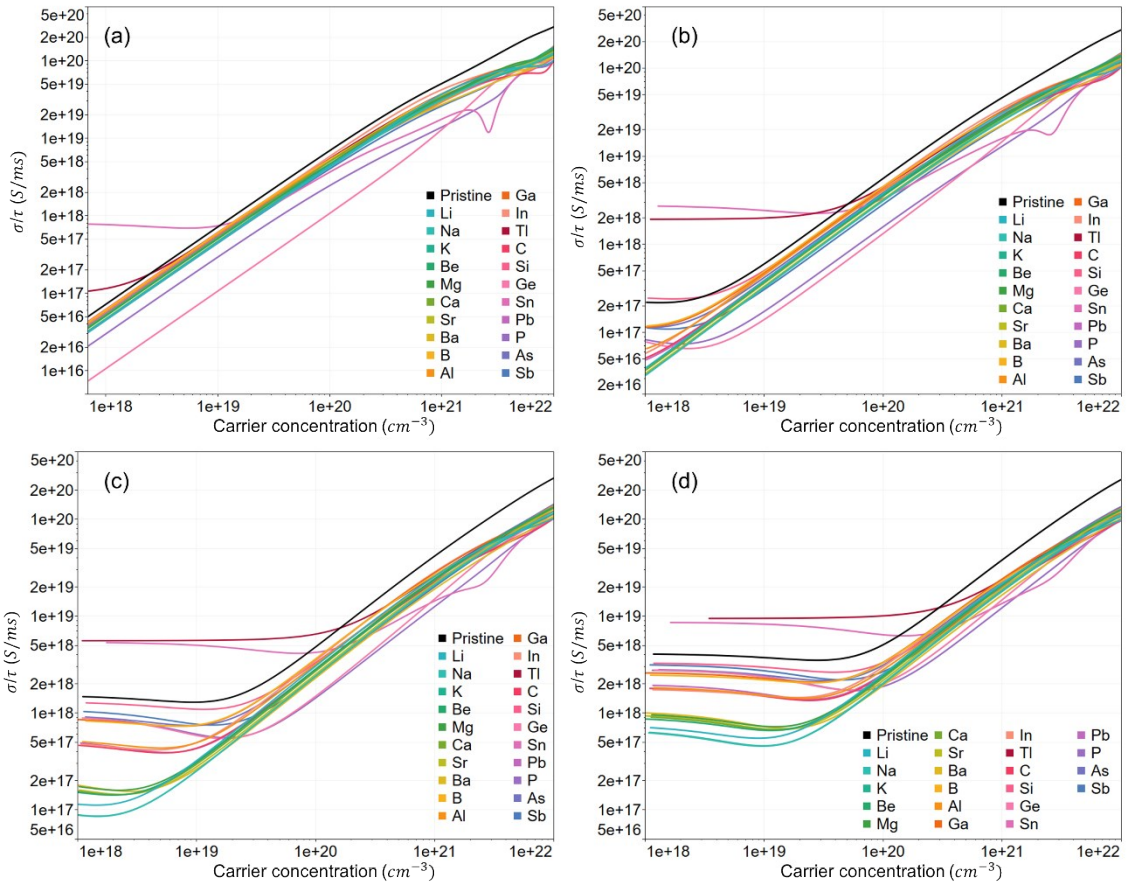

Figure 5. The calculated electrical conductivity relative to relaxation time for pristine Bi_2O_2Se and p-doping cases with temperatures of (a) 300K (b) 600K (c) 900K (d) 1200K.

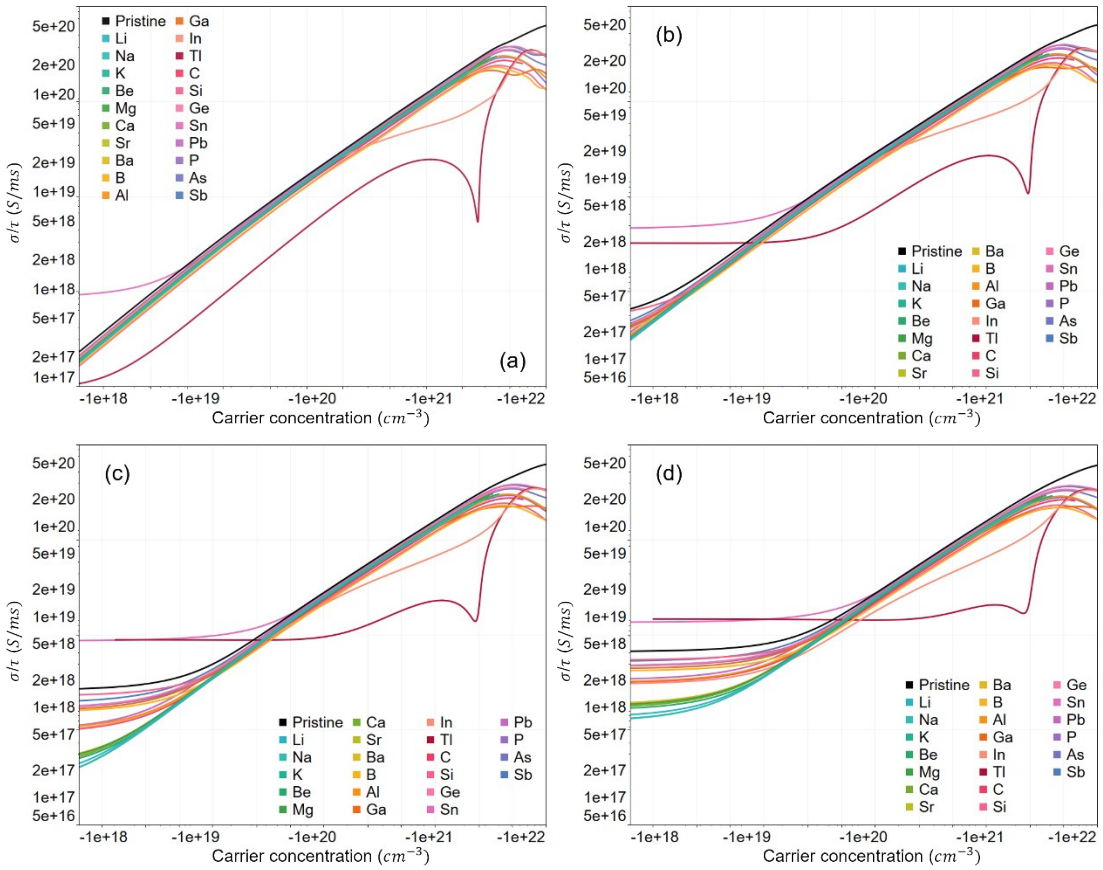

Figure 6. The calculated electrical conductivity relative to relaxation time for pristine Bi2O2Se and n-doping cases with temperatures of (a) 300K (b) 600K (c) 900K (d) 1200K.

5. Calculated Seebeck coefficient

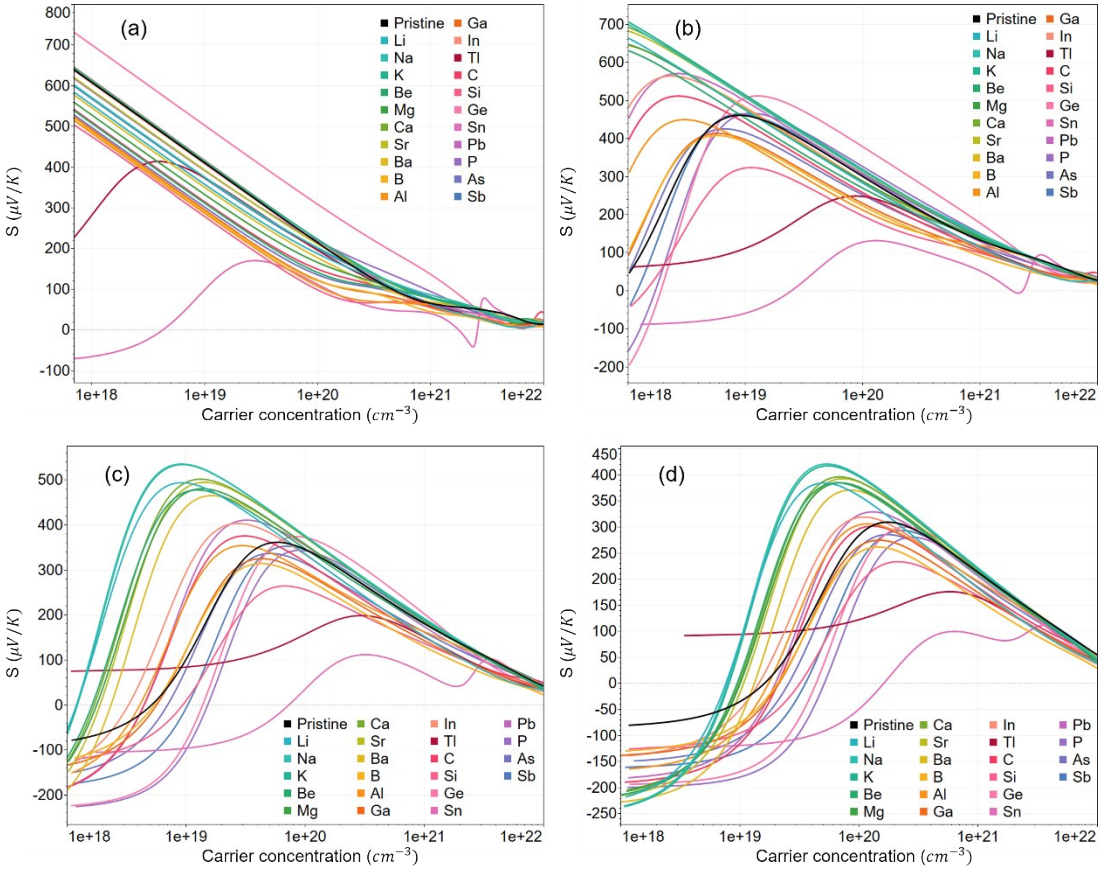

Figure 7. The calculated Seebeck coefficient for pristine Bi_2O_2Se and p-doping cases with temperatures of (a) 300K (b) 600K (c) 900K (d) 1200K.

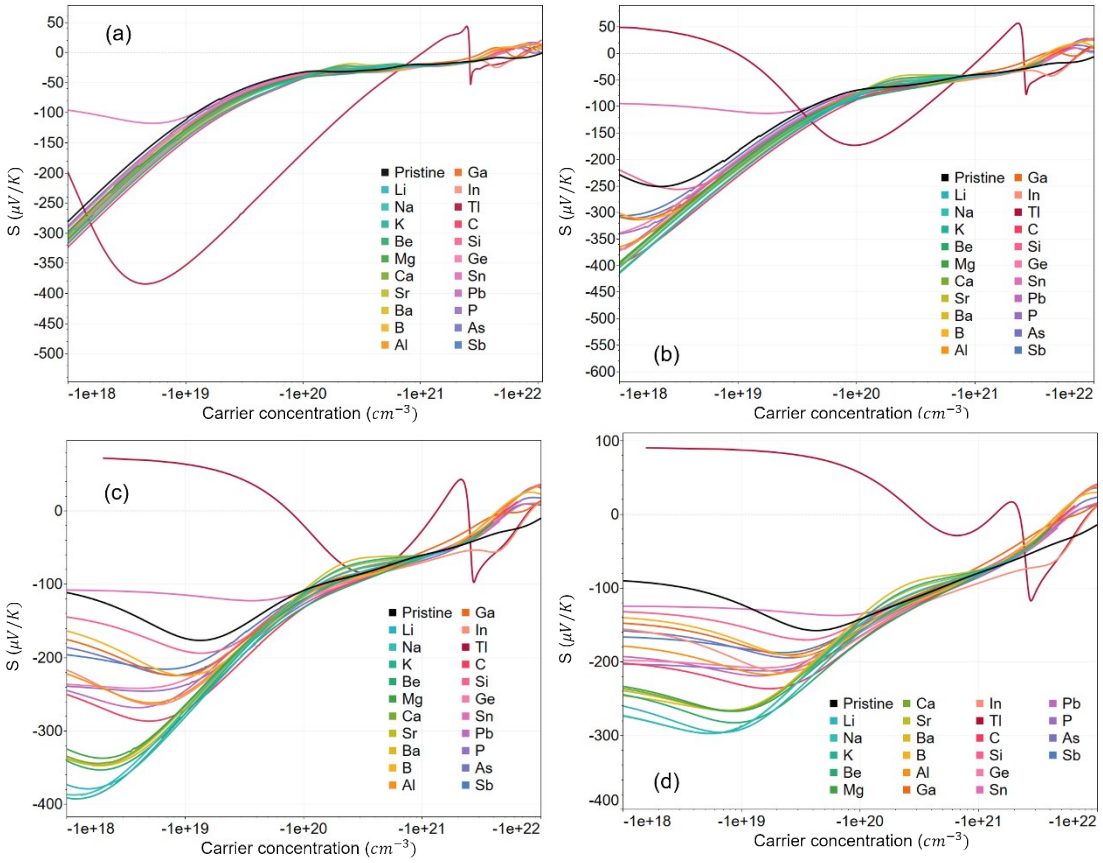

Figure 8. The calculated Seebeck coefficient for pristine Bi_2O_2Se and n-doping cases with temperatures of (a) 300K (b) 600K (c) 900K (d) 1200K.

6. Calculated power factor

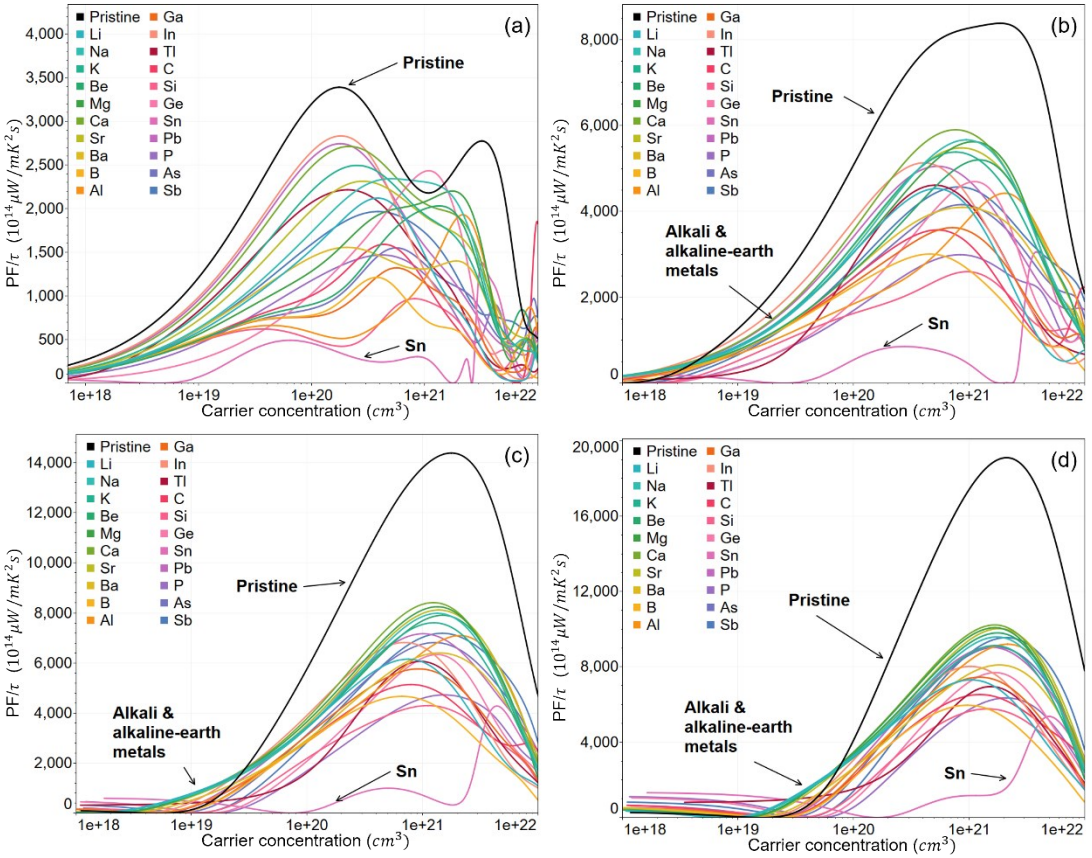

Figure 9. The calculated power factor relative to relaxation time for pristine Bi_2O_2Se and p-doping cases with temperatures of (a) 300K (b) 600K (c) 900K (d) 1200K.

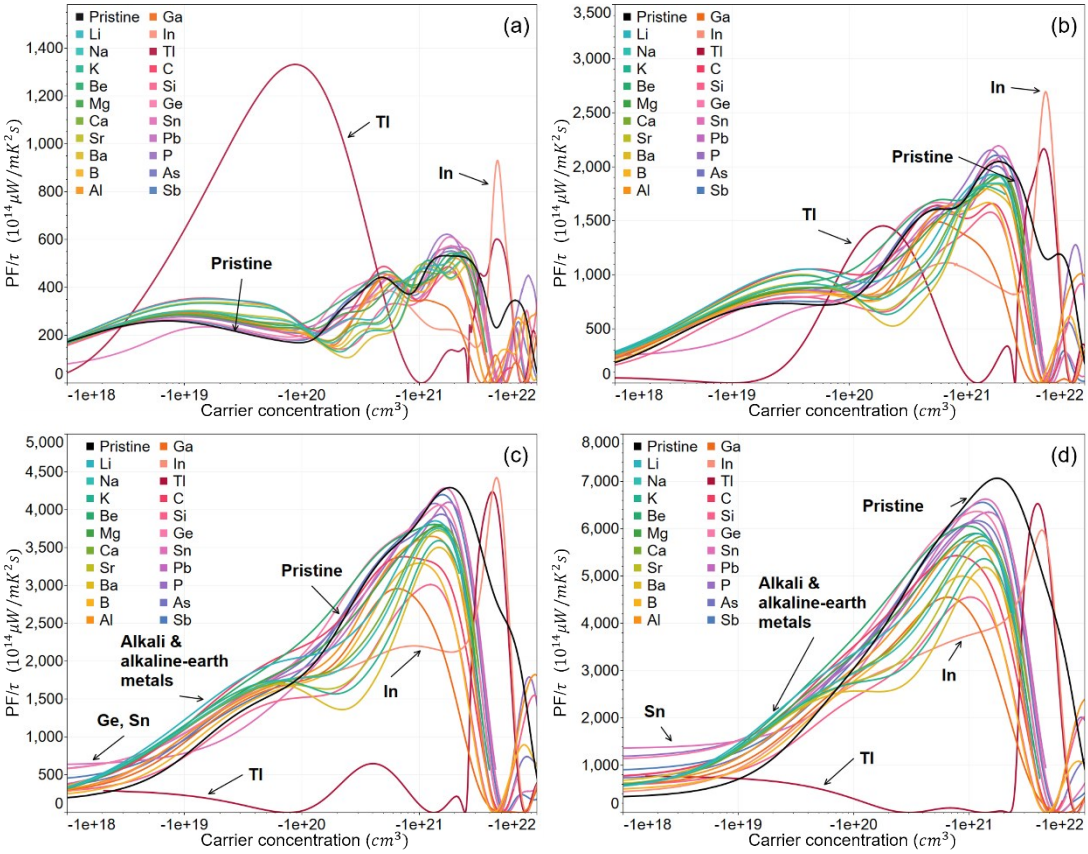

Figure 10. The calculated power factor relative to relaxation time for pristine Bi_2O_2Se and n-doping cases with temperatures of (a) 300K (b) 600K (c) 900K (d) 1200K.

Reference:

[1] C. Wang, G. Ding, X. Wu, S. Wei and G. Gao, New Journal of Physics, 2018,20, 123014

[2] D. Guo, C. Hu, Y. Xi and K. Zhang, The Journal of Physical Chemistry C, 2013,117, 21597–21602.

[3] X.-L. Zhu, P.-F. Liu, G. Xie and B.-T. Wang, Physical Chemistry Chemical Physics, 2019,21, 10931–10938.

[4] J. Wu, H. Yuan, M. Meng, C. Chen, Y. Sun, Z. Chen, W. Dang,C. Tan, Y. Liu, J. Yin et al., Nature nanotechnology, 2017,12,530–534

[5] P. Ruleova, C. Drasar, P. Lostak, C.-P. Li, S. Ballikaya andC. Uher, Materials Chemistry and Physics, 2010,119, 299–302.

[6] P. Ruleová, T. Plechacek, J. Kasparova, M. Vlcek, L. Benes,P. Lostak and C. Drasar, Journal of Electronic Materials, 2018,47, 1459–1466.

[7] B. Zhan, S. Butt, Y. Liu, J.-L. Lan, C.-W. Nan and Y.-H. Lin, Journal of Electroceramics, 2015,34, 175–179

[8] Zhan, Y. Liu, X. Tan, J.-l. Lan, Y.-h. Lin and C.-W. Nan, Journal of the American Ceramic Society, 2015,98, 2465–2469.

[9] B. Zhan, Y. Liu, J. Lan, C. Zeng, Y.-H. Lin and C.-W. Nan, Materials, 2015,8, 1568–1576.

[10] R. Liu, X. Tan, Y. Liu, G. Ren, C. Liu, Z. Zhou, C. Nan, Y. Lin et al., Journal of the European Ceramic Society, 2018,38,2742–2746.

[11] X. Tan, J.-L. Lan, Y.-C. Liu, G.-K. Ren, C.-C. Zeng, Y.-H. Lin and C. Nan, Journal of Electroceramics, 2016,37, 66–72.

[12] X. Tan, Y. Liu, R. Liu, Z. Zhou, C. Liu, J.-L. Lan, Q. Zhang, Y.-H. Lin and C.-W. Nan, Advanced Energy Materials, 2019,9,1900354.

[13] X. Tan, J.-l. Lan, G. Ren, Y. Liu, Y.-H. Lin and C.-W. Nan, Journal of the American Ceramic Society, 2017,100, 1494–1501.

[14] . Tan, Y. Liu, K. Hu, G. Ren, Y. Li, R. Liu, Y.-H. Lin, J.-L. Lan and C.-W. Nan, Journal of the American Ceramic Society, 2018,101, 326–333.

[15] X. Tan, J.-L. Lan, K. Hu, B. Xu, Y. Liu, P. Zhang, X.-Z. Cao, Y. Zhu, W. Xu, Y.-H. Lin et al., Journal of the American Ceramic Society, 2018,101, 4634–4644